Materials Today Bio 32 (2025) 101690

Contents lists available at ScienceDirect

Materials Today Bio

journal homepage: www.journals.elsevier.com/materials-today-bio

Peptide loaded self-healing hydrogel promotes diabetic skin wound healing through macrophage orchestration and inflammation inhibition

Ziyi Lu [a,b,1], Kaijia Tan [a,b,1], Shuwen Xiang [a,b], Yuchen Zhang [a,b], Fangliang Luo [a,b], Xingdan Liu [a,b,*], Xiaoli Zhao [c,**], Liping Ouyang [a,b,***]

[a] Shanghai Key Laboratory of Flexible Medical Robotics, Tongren Hospital, Institute of Medical Robotics, Shanghai Jiao Tong University, Shanghai, China
[b] Hongqiao International Institute of Medicine, Tongren Hospital, Shanghai Jiao Tong University School of Medicine, Shanghai, 200336, China
[c] Research Center for Human Tissues and Organs Degeneration, Shenzhen Institute of Advanced Technology, Chinese Academy of Sciences, Shenzhen, 518055, China

ARTICLE INFO

Keywords:
Peptide
Anti-inflammation
Chronic diabetic wound repair
Hydrogel

ABSTRACT

Chronic wound is one of the complications of diabetes, and its difficult cure results in increased disability rate and mortality rate, which brings serious psychological and economic burden to patients. Excessive inflammation is one of the key reasons for poor tissue healing in chronic diabetic wounds. Herewith, the development of wound dressings with anti-inflammation and promoting tissue repair is of great significance for the treatment of chronic diabetic wounds. In this work, the Ac2-26 (Ac) peptide was loaded into the hyaluronic acid (HA) complex hydrogel for diabetic wound therapy. The hydrogel containing Ac had good mechanical properties, self-healing properties, and adhesion. It could down-regulate the M1/M2 phenotype of macrophages effectively, thereby promoting collagen type III (COL-III) secretion and migration of L929 and angiogenesis of HUVECs. Furthermore, the hydrogel containing Ac could restore the oxidative phosphorylation process and down-regulated toll-like receptor signaling pathway and inflammatory gene expression in the pathological environment of diabetes, showing a superior anti-inflammatory effect to ultimately promote the collagen deposition and angiogenesis in tissues for wounds repair. The HA complex hydrogel containing Ac demonstrated a good potential for clinical application in diabetic wound repair.

1. Introduction

The difficulty of diabetic chronic wound healing is one of the clinical issues, which urgently needs to be addressed due to that diabetic chronic wound often causes serious consequences, such as amputation [1,2]. In the diabetic wound, the high glucose microenvironment often induces the accumulation of advanced glycation end products (AGEs), which leads to the difficulty of vascular regeneration and slows wound healing [3,4]. Wound repair is a complex and orderly biological process, which mainly includes three stages: inflammation, cell proliferation, and tissue remodeling [5]. Among them, excessive inflammation is an important reason that hinders the healing of diabetic wounds [6]. Macrophages are highly plastic immune cells that play a pivotal role in the inflammatory response [7]. Its functional phenotypes mainly include pro-inflammatory M1 type and anti-inflammatory M2 type [8]. In pathological situations, hyperglycemia and the formation of AGEs impede macrophages-mediated phagocytosis of apoptotic cells, thus generating a sustained pro-inflammatory response and recruiting other inflammatory cells to directly or indirectly destroy the surrounding tissue [9,10]. Therefore, promoting transformation of macrophages into anti-inflammatory M2 type is an effective strategy to accelerate the healing of diabetic chronic wounds.

Compared with chemical drugs, peptide drugs have the advantages of high biological activity, strong specificity, and fewer side effects. They are rich in species and play a variety of biological functions such as immune regulation and tissue repair, thereby being utilized in research

* Corresponding author. Shanghai Key Laboratory of Flexible Medical Robotics, Tongren Hospital, Institute of Medical Robotics, Shanghai Jiao Tong University, Shanghai, China.
** Corresponding author.
*** Corresponding author. Shanghai Key Laboratory of Flexible Medical Robotics, Tongren Hospital, Institute of Medical Robotics, Shanghai Jiao Tong University, Shanghai, China.
E-mail addresses: liuxd_cumt@126.com (X. Liu), zhao.xl@siat.ac.cn (X. Zhao), lpouyang@shsmu.edu.cn (L. Ouyang).
[1] These authors contributed equally.

https://doi.org/10.1016/j.mtbio.2025.101690
Received 31 December 2024; Received in revised form 6 February 2025; Accepted 19 March 2025
Available online 20 March 2025

on diabetes, cardiovascular diseases, neurodegenerative diseases, and other clinical problems [11–13]. Yang et al. identified a new active peptide molecule RL-QN15 derived from the skin of the amphibian frog from Yunnan Province, which can activate macrophages to release TGF-β1, thereby promoting epidermal cell migration, granulation tissue regeneration, and epidermal reconstruction that further contributes to skin tissue regeneration [14]. Cao et al. combined antimicrobial peptide (LL-37) and anti-inflammatory peptide (C15) sequences to prepare bifocal polypeptides to disrupt bacterial membrane formation and reduce the release of pro-inflammatory cytokine, which has been used in the treatment of periodontitis [15]. However, peptide drugs are often unstable in physical and chemical properties. Characterized by their susceptibility to oxidation, hydrolysis, aggregation, and poor cellular membrane permeability, these peptides have a short half-life, rapid clearance rate and oral bioavailability constraints [16–18].

Hydrogel is a good carrier for drug delivery and an effective dressing for wound treatment due to its unique three-dimensional network structure, high water content, suitable mechanical strength, and degradability [19–21]. Hyaluronic acid (HA) is a natural polysaccharide, which is widely used in the preparation of biomimetic hydrogel because of its good hydrophilicity, excellent biocompatibility and biodegradability, as well as rich biological functions including anti-inflammation, anti-wrinkle, and skin wound healing properties [22–24]. However, the natural hydrogel based on HA still have some deficiencies, including insufficient mechanical strength and susceptibility to enzymatic hydrolysis [25,26]. β-Cyclodextrin (β-CD) is a biosafe cyclic oligosaccharide and can assist drug delivery. It not only has a unique internal hydrophobic and external hydrophilic spatial structure, but also provides a rich conjugated chemical environment, which can increase the stability of drug loading, improve the dissolution and bioavailability of drugs, and reduce its toxic side effects [27,28]. Herewith, it is of great significance to enhance the mechanical properties of hydrogel and the loading stability of polypeptide drugs though addition of multiple components to HA for the treatment of diabetic chronic wounds.

Consequently, in this study, HA and β-CD were mixed and loaded with different concentrations of Ac polypeptide drugs. Biocompatible polyvinyl alcohol (PVA) and polyethylene glycol (PEG) were added to HA to enhance its gel-forming properties as described in the previous work, thereby constructing polypeptide complex hydrogel [29]. The immunomodulatory and tissue repair capabilities of polypeptide complex hydrogel were investigated *in vitro*, in zebrafish models, and in diabetic wound models. RNA sequencing (RNA-Seq) was used to further analyze the mechanisms through which hydrogel regulate inflammation and promote wound healing.

2. Methods

2.1. Preparation of hydrogel

The 1.5 g of PVA (P139546, Aladdin) was solubilized in 15 mL sterilized water with stirring at 90 °C to create a 100 mg/mL PVA solution. Ac (HY-P1098A, Med Chem Express) was dissolved in sterilized water at room temperature with different concentrations of 0 μg/mL, 0.6 μg/mL, 1.2 μg/mL, and 1.8 μg/mL, respectively. Subsequently, 15 mg of β-CD (C118530, Aladdin), 150 mg of HA (H107141, Aladdin), and 150 mg of PEG (P103734, Aladdin) were dissolved in 6 mL of the above Ac solution. Ac mixture and PVA solution were rapidly mixed with a volume ratio of 1:2 to prepare the polypeptide complex hydrogel. Then, these hydrogels were subjected to freeze-thawing at −20 °C for more than 12 h. With the increase of Ac content, the obtained hydrogels are successively named Ac0, AcL, AcM, and AcH.

2.2. Characterization of hydrogel

The rheological experiments were measured at using a rheometer (MCR 102e, Anton Parr, AUT). The Ac0 hydrogel was loaded on the parallel plate with a diameter of 25 mm. The G′ and G″ were examined by time sweep tests at 1 % strain and 1 Hz frequency. The frequency sweep tests (0.1–100 rad/s) were studied at a constant strain of 1 % and a frequency of 1 Hz. The shear thinning test was performed as the shear rate increased from 0.1 to 1000 s^{-1}. The strain scanning was conducted over a strain range of 0.01 %–1000 %. The oscillatory strain scanning tests were measured with alternating 500 % strain and 1 % strain at a constant angular frequency of 1 rad/s.

The hydrogel was cut into two parts and colored orange and green pigment, respectively. Then, the two parts were reconnected at room temperature to evaluated the self-healing ability of hydrogel. In addition, the hydrogel was attached to the knuckle and bent at different angles to observe its adhesion.

2.3. Cell response in vitro

2.3.1. Cell culture

Macrophages (RAW 264.7, SCSP-5036, Cell Bank), mouse fibroblasts (L929, SCSP-5039, Cell Bank), and human umbilical vein endothelial cells (HUVECs, YPC-H001, Science Cell) were used in this study. Macrophages were cultured in Dulbecco's modified eagle medium (C11995500BT, Gibco) supplemented with 10 % fetal bovine serum (A5669701, Gibco) and 1 % penicillin/streptomycin (CB010, EpiZyme). L929 cells were cultured in Minimun Essential medium (C12571500BT, Gibco) supplemented with 10 % fetal bovine serum (A5669701, Gibco) and 1 % penicillin/streptomycin (CB010, EpiZyme). HUVECs were cultured in Endothelial cell medium (1001, Science Cell). The above cells were cultured in an incubator at 37 °C with 5 % humidity.

2.3.2. Cell proliferation

Macrophages were seeded in 12-wells plates at a density of 1×10^5 cells/well. Subsequently, the pre-swollen hydrogels were placed in the upper chamber with 3 μm pore size filters of the transwell to co-culture with the cells. After further incubation for 1 and 4 days, cell activity assays were performed with Alamar Blue™ HS Cell Viability Reagent (A50101, Thermo Scientific). L929 cells were seeded in 12-wells plates at a density of 2×10^4 cells/well. Subsequently, the pre-swollen hydrogels were placed in the upper chamber with 3 μm pore size filters of the transwell to co-culture with the cells. After further incubation for 1, 4 and 7 days, cell activity assays were performed with Alamar Blue™ HS Cell Viability Reagent.

2.3.3. Enzyme-linked immunosorbent assay test

The expression levels of inflammation-related cytokines in macrophages after culture with hydrogel for 4 days were detected through Mouse TNF-α ELISA Kit (MEC1003, Anagen), Mouse IL-1β ELISA Kit (MEC1010, Anagen), Mouse IL-10 ELISA Kit (A1010A0210, BioTNT), and Mouse TGF-β1 ELISA Kit (MEC1012, Anagen), respectively.

2.3.4. Immunofluorescence staining of cells

In 12-wells plates, macrophages were planted onto cell crawls at a density of 1×10^5 cells/well and LPS (10 ng/mL) was added for inflammatory stimulation. Subsequently, pre-swollen hydrogels were placed in the upper chamber with 3 μm pore size filters of the transwell to co-culture with the cells. After days 1 and 4, cells were fixed using 4 % paraformaldehyde, and immunofluorescence staining was performed with primary antibodies, anti-CD206 antibody (NBP1-90020, Novus, 1:200) and anti-CCR7 antibody (NB100-712SS, Novus, 1:200), and second antibodies, Alexa 488-conjugated anti-rabbit antibody (ab150073, Abcam, 1:400), and Alexa 594-conjugated anti-Goat antibody (ab150132, Abcam, 1:400) to label M1-type and M2-type macrophages. In addition, anti-NLRP3 Rabbit pAb (GB114320, Servicebio, 1:200), and Alexa Fluor 488 conjugated goat anti-rabbit IgG (GB25303, Servicebio, 1:400) were used to detect the expression of the inflammatory factor NLRP3 in macrophages.

Macrophages were seeded in 12-wells plates at a density of 1×10^5

cells/well. Subsequently, the pre-swollen hydrogels were placed in the upper chamber with 3 μm pore size filters of the transwell to co-culture with the cells. After further incubation for 4 days, the supernatant was collected as a conditioned medium. The conditioned media for the subsequent experiments were based on this. L929 cells were inoculated on the cell crawls in 24 wells at a density of 2×10^4 cells/well. The conditioned medium collected above was co-cultured with the cells on day 4 of culture by diluting it 1:1 with fresh medium. After further incubation for 3 days, the cells were fixed using 4 % paraformaldehyde, and COL-III immunofluorescence staining was performed using anti-COL-III Rabbit pAb (GB111629, Servicebio, 1:200) and Alexa Fluor 488 conjugated goat anti-rabbit IgG H&L (GB25303, Servicebio, 1:50). The cell fluorescence images were observed under laser confocal microscope (TCS SP8, Leica).

L929 cells were seeded at a density of 2×10^5 cells/well into the 12-wells plates. After culture for 24 h, the cells were scratched by the pipette tip, and washed with phosphate buffered saline (PBS) before adding conditioned medium. The L929 migration was observed and photographed under a fluorescence microscope (TS2-S-SM, Nikon) after another 24 h. The migration rate was analyzed by the ImageJ software.

2.3.5. *In vitro tube formation assay*

200 μL of Matrigel was added to the pre-cooled 24-wells plates and cured at 37 °C for 1 h. HUVECs were then seeded at a density of 5×10^4 cells/well. After 6 h of co-culture with conditioned medium, the tube formation was observed with a fluorescence microscope (TS2-S-SM, Nikon), and the number of branch points and the tube length were analyzed by ImageJ software.

2.4. *Zebrafish tail-breaking model*

The experimental protocol concerning animals used in this study was approved by the Shanghai Tongren Hospital Ethics Committee (2024-184). The wild-type AB and the transgenic zebrafish line Tg (mpeg1: mCherry) were used to observe the inflammatory response *in vivo*. Reduction of pigmentation in zebrafish embryos by adding 0.003 % 1-phenyl-2-thiourea to the culture medium at 12 h after fertilization. A tail-breaking model was created by creating a local injury in the caudal fin of a zebrafish larva at 3 days postfertilization. Recruitment of fluorescently labeled macrophages (red) at the wound site was observed after co-culture with the pre-swollen hydrogels for 8 and 24 h.

2.5. *Diabetic chronic wound model*

The experimental protocol concerning animals used in this study was approved by the Shanghai Tongren Hospital Ethics Committee (2021-090-01). Male SD rats of 6–8 weeks were used to create a diabetic chronic wound model. The rats were injected once with Streptozocin (STZ) solution (s8050, Solarbio, 65 mg/kg) through the intraperitoneal injection. Blood glucose levels in rats were measured 5 days after drug induction. The rats with blood glucose levels ≥16.7 mmol/L accompanied by symptoms of polydipsia, polyphagia, polyuria, and weight loss were considered to be successfully modeled. Afterwards, the rats were anesthetized using 1 % sodium pentobarbital, and the dorsal region of the rats was depilated and disinfected before a piece of skin tissue with a diameter of 20 mm was excised in the dorsal skin of the rats to construct the diabetic chronic wound. It should be noted that a dressing was used to fix the hydrogel at the wound site and the hydrogel was added on day 0 without any changes during the experiments. The experimental group was covered with pre-swollen Ac0, AcL, AcM, and AcH hydrogels, and the Control group was covered with gauze.

To evaluate the macroscopic wound healing effect of hydrogel, the wound pictures at 0, 3, 7, and 14 days were measured and photographed. For histological analysis, wound tissues were collected and immersed in 4 % paraformaldehyde for fixation at days 7 and 14. The fixed tissue was then embedded in paraffin and sectioned. Immunofluorescence staining was performed with anti-CD68 antibody (GB113109, Servicebio, 1:3000), anti-CD206 antibody (GB113497, Servicebio, 1:5000), anti-iNOS antibody (GB11119, Servicebio, 1:1000), Cy3 conjugated goat anti-rabbit IgG (GB21303, Servicebio, 1:300), Alexa Fluor 488 conjugated goat anti-rabbit IgG (GB25303, Servicebio, 1:400), and Cy5 conjugated goat anti-rabbit IgG (GB27303, Servicebio, 1:400) to label M1-type and M2-type macrophages. Immunohistochemical staining was performed with anti-CD31 antibody (GB113151, Servicebio, 1:500) and HRP conjugated goat anti-rabbit IgG (H + L) (GB23303, Servicebio, 1:200). In addition, the slices were also stained with HE and Masson. These slices were scanned by NanoZoomer S60 (Hamamatsu, Japan) and Pannoramic 250 FLASH (3DHISTECH, Hungary), respectively.

2.6. *RNA sequencing (RNA-Seq)*

The collected rat skin tissues were immediately placed in freeze-dried tubes and stored at −80 °C for subsequent experiments. Total RNA was extracted using TRIzol reagent following the instructions. RNA purity was identified and quantified using a NanoDrop 2000 spectrophotometer (Thermo Scientific, USA) and RNA integrity was assessed using an Agilent 2100 Bioanalyzer (Agilent Technologies, USA). Transcriptome libraries were constructed using the VAHTS Universal V5 RNA-Seq Library Prep Kit according to the instructions. The libraries were sequenced using the llumina Novaseq 6000 sequencing platform. Differentially expressed genes were analyzed using DESeq2 software. The thresholds for differentially expressed genes (DEGs) were $q < 0.05$ and foldchange >2 or foldchange <0.5. Subsequently, differentially expressed genes were analyzed for GO, KEGG Pathway, Reactome and WikiPathways enrichment and screened for significantly enriched terms using R (v 3.2.0). The transcriptome sequencing and analysis were performed by OE Biotech Co., Ltd. (Shanghai, China).

2.7. *Quantitative RT-PCR*

The above extracted RNA was reversely transcribed into cDNA using a reverse transcription kit (A2010A0601, Biotnt), and the real-time polymerase chain reaction (RT-PCR) was performed on ABI ViiA7 with Realtime PCR PreMIX (A2010A001, Biotnt). The expressions of TNF-α and IL-1β were analyzed by the $2^{-\Delta\Delta CT}$ approach. β-Actin was used as the internal reference gene.The primer sequences for qPCR were shown in Table S1.

2.8. *Statistical analysis*

GraphPad Prism (Version 8.0, GraphPad Soft-ware, USA) was used for data analysis. Quantitative data were expressed as mean ± standard deviation (SD). One-way ANOVA analysis, two-way ANOVA analysis and Tukey's multiple comparison tests were used to analyze the significant differences. *$p < 0.05$, **$p < 0.01$ ***$p < 0.001$ and ****$p < 0.0001$.

3. Results

3.1. *Characterization of hydrogel*

The three-dimensional structure of hydrogel was observed using scanning electron microscopy. As shown in Fig. 1a, all groups of hydrogels presented an irregular porous network structure, which facilitated adequate air and drug permeability. The FTIR spectra of the samples were shown in Fig. 1b. Compared with Ac0, the characteristic peaks of C-N appeared at about 1170 cm^{-1} in the AcL, AcM, and AcH. Moreover, an enhancement of the amide bond at 1364 cm^{-1} could be observed with increased Ac content in the hydrogel. These results demonstrated that Ac was successfully loaded into the hydrogel system. The storage modulus (G′) and the loss modulus (G″) of the Ac0 hydrogel

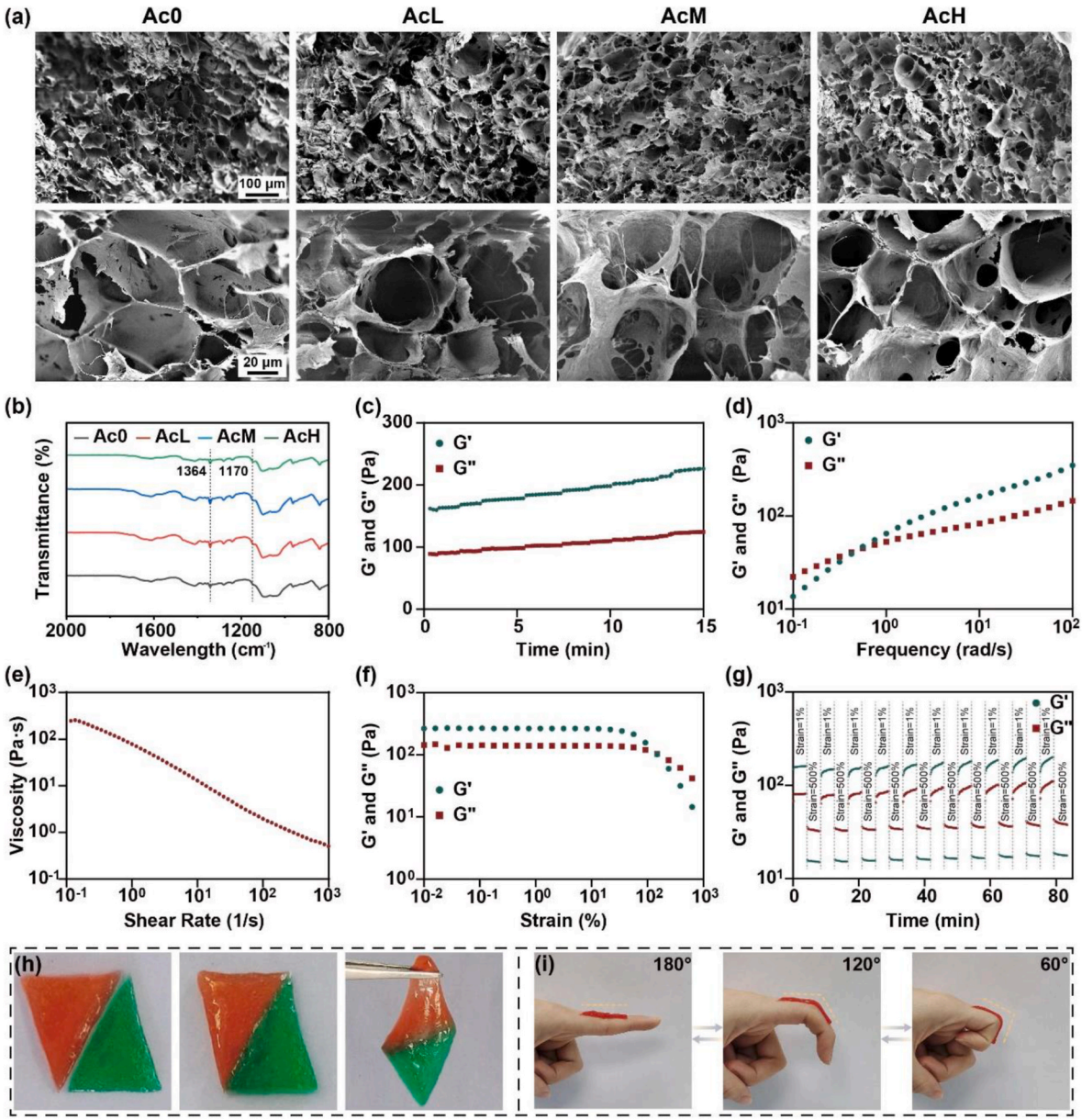

Fig. 1. Characterization of the hydrogel systems. (a) Cross-section morphologie of Ac0, AcL, AcM, and AcH hydrogels after freeze-drying. (b) FTIR spectra of Ac0, AcL, AcM, and AcH hydrogels. (c) The change of storage modulus (G′) and loss modulus (G″) under 15 min test. (d) Frequency sweep measurement of the hydrogel. (e) Shear-thinning properties of the hydrogel. (f) The strain sweep measurements of the hydrogel. (g) Rheological properties of the hydrogel at the alternate step strain from 1 % to 500 % for ten cycles. (h) Self-healing properties of the hydrogel. (i) Adhesion properties of the hydrogel.

were evaluated via rheological tests. The G′ values of the Ac0 hydrogel were consistently higher than the G″ values during the test period, indicating the formation of a stable gel state (Fig. 1c). With the increase of frequency, the G′ < G″ of Ac0 changed to G′ > G″, indicating that the hydrogel could change from sol to gel state at a high frequency of 0.422 rad/s (Fig. 1d). The shear-thinning property test of the Ac0 was performed, and the results were shown in Fig. 1e. It was illustrated that the hydrogel was injectable and could be adapted to different shapes, thereby facilitating the application of wounds with irregular contours. The strain scanning tests determined that the hydrogel network collapsed at 148 % strain (Fig. 1f). The stability of the hydrogel was tested in the strain amplitude sweep tests at 25 °C, and the results were shown in Fig. 1g. The Ac0 hydrogel was destroyed at 500 % of strain, and when the applied strain was returned to 1 %, the hydrogel rapidly recovered to a gel state. It could go through at least 10 cycles, indicating that the hydrogel could rapidly self-heal even after damage. The macroscopic self-healing ability of the hydrogel was further evaluated. As shown in Fig. 1h, the hydrogel was stained with two dyes, orange and green, and contacted together without any external stimuli. The hydrogel healed in 30 min and could be lifted with tweezers without splitting. Moreover, the Ac0 hydrogel could be adhered to the finger joints for adaptive movement without falling off, showing its good adhesion properties (Fig. 1i). In addition, the release of the complex hydrogel system was evaluated using FITC as a model drug. Fig. S1 showed that the complex hydrogel system exhibited a law of slow and sustained release, and the drug release increased with the increase of drug loading concentration.

3.2. Macrophage response of hydrogel

The biocompatibility of hydrogel with the murine-derived macrophages and the modulation of the inflammatory response to

macrophages *in vitro* were investigated under stimulation of lipopolysaccharides (LPS) of 10 ng/mL. All groups of hydrogels exhibited good biocompatibility to macrophages (Fig. S2). The expression of CD206 and CCR7 in macrophages of each group was visualized using immunofluorescence staining, with CD206 (green) and CCR7 (red), respectively. The immunofluorescence images and corresponding quantitative results in each group at 1 day were shown in Fig. 2a–c. It could be observed that the green fluorescence and red fluorescence in the AcM group were slightly brighter than the other four groups. The immunofluorescence images and corresponding quantitative results in each group on day 4 were shown in Fig. 2d–f. The pro-inflammatory phenotypic marker CCR7 was maintained at a high level in the Control group on day 4, while the expression of CCR7 was significantly reduced and the expression of the anti-inflammatory marker CD206 was markedly increased in hydrogel-treated macrophages. Furthermore, the expression levels of cytokines secreted by macrophages in each group were also examined. As shown in Fig. 2g–j, LPS-stimulated macrophages expressed excessive amounts of TNF-α and IL-1β. The expression of pro-inflammatory cytokines was inhibited to varying degrees after co-culture with hydrogel, and the inhibition was approximately significant with increased Ac content. The expression of anti-inflammatory cytokines IL-10 and TGF-β1 showed an increasing trend in the hydrogel groups, and the expression increased with the increment of Ac loading. The above data suggested that the AcM and AcH hydrogels were effective in suppressing inflammation.

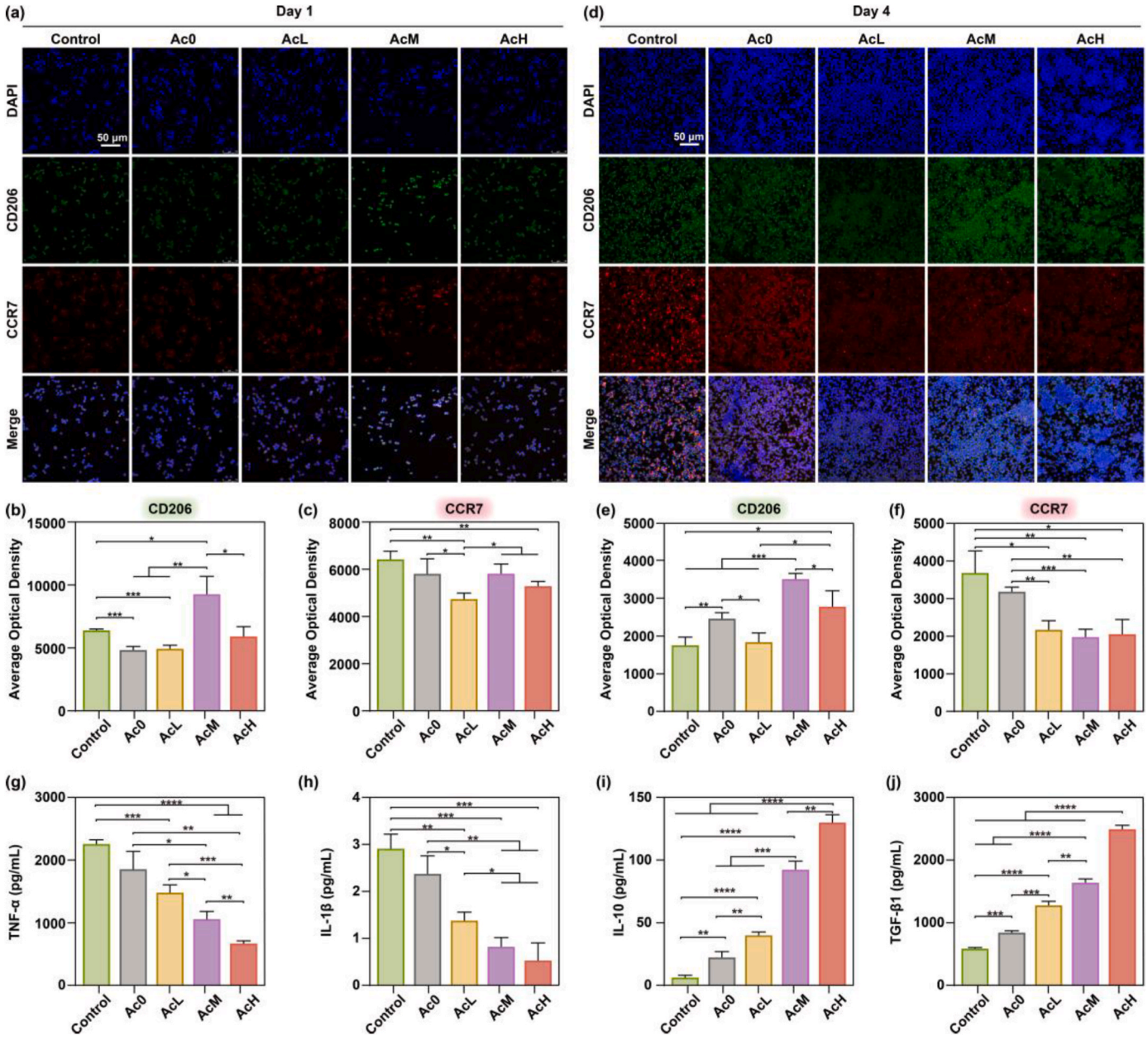

Fig. 2. Effects of hydrogel on macrophage polarization *in vitro*. (a) Representative fluorescence images of the macrophage phenotypes in each group on day 1 with LPS stimulation. M2 macrophages were marked with CD206 (green). M1 macrophages were marked with CCR7 (red). Nuclei was marked with DAPI (blue). The average optical density of CD206 (b) and CCR7 (c) in macrophages on day 1 with LPS stimulation. (d) Representative fluorescence images of the macrophage phenotypes in each group on day 4 with LPS stimulation. The average optical density of CD206 (e) and CCR7 (f) in macrophages on day 4 with LPS stimulation. (g) Expression levels of inflammatory cytokines of macrophages in each group on day 4. Data were presented by mean ± SD, n = 3. P value was calculated by one-way ANOVA. *p < 0.05, **p < 0.01, ***p < 0.001, ****p < 0.0001.

3.3. Cells behavior cultured with conditional medium

All groups of hydrogels showed great biocompatibility to L929 (Fig. S3). The supernatant of hydrogel incubated with macrophages for 4 days was used as the conditioned medium. The collagen type III (COL-III) secretion of L929 in each group was detected under conditioned medium and the results were shown in Fig. 3a and b. Compared with the Control group, COL-III secretion of L929 increased in the hydrogel groups, among which COL-III secretion of L929 was significantly improved in the Ac-containing hydrogel groups. The effect of hydrogel on cell migration was examined by scratch assay. As shown in Fig. 3c and d, hydrogel boosted the migration of L929 and accelerated the closure of the cell-free gap compared with the Control group, especially in the AcM group. In addition, the effect of the samples on the angiogenic potential of HUVECs was assessed by tubule formation experiments (Fig. 3e). The number of branch points and the total tube length were used to evaluate the formed tube network (Fig. 3f and g). Compared with the Control group, the HUVECs in hydrogel groups showed enhanced activity in neointimal formation. Significantly, The number of branch points and the tube length were substantially increased in the AcM and AcH groups compared with the Ac0 and AcL groups. These results demonstrated that the AcM and AcH hydrogels could promote the COL-III secretion, migration of L929 and the angiogenesis of HUVECs after regulating the macrophages.

3.4. Inflammatory response of hydrogel in zebrafish tail-breaking model

The inflammatory regulation by hydrogel *in vivo* was evaluated in a tail-breaking model constructed from zebrafish genetically tagged with macrophages (Tg (mpeg1: mCherry)). Fig. 4a depicted the experimental process of co-culture with hydrogel after tail-breaking at the caudal fin site of zebrafish on day 3 post-fertilisation. As shown in Fig. 4b and c, there was not any significant change in the number of inflammatory cells in the Ac0 group compared with the Control group after co-culture with hydrogel for 8 h, while the number of inflammatory cells in the Ac-containing hydrogel groups decreased remarkably. Furthermore, AcM and AcH groups still could significantly inhibit the excessive inflammation in the zebrafish tail-breaking model compared with the Control and Ac0 groups, which had continuously enhanced inflammation after culture for 24 h (Fig. 4d and e). These results indicated the AcM and AcH hydrogels effectively alleviated inflammation *in vivo*.

3.5. Ac-containing hydrogel promoted diabetic wound healing

The experimental processes of diabetic wound model were shown in Fig. 5a. The rat diabetic model was successfully induced via intraperitoneal injection of Streptozocin (STZ). The blood glucose value of the rats was measured for 5 days after the injection, and the model was successfully constructed with the value exceeding 16.7 mmol/L. The skin defects (Φ 20 mm) were created on the back of the rats and treated with gauze, Ac0, AcL, AcM and AcH hydrogels, respectively. These wounds were photographed on days 0, 3, 7, and 14 to observe the progress of repair. As shown in Fig. 5b, the wound area decreased in all groups over time, as evidenced by the fact that the area of wound defects in the AcM and AcH groups was smaller than that in the other three groups on day 14, and dark blood scabs were still evident in the Control group. In addition, the wound healing process schematic and wound healing rate statistics showed that wound healing rate in the AcM and AcH groups was significantly faster than that in the other three groups. The wound remained optimal at day 14 with a healing rate of 90.15 ± 0.6 % and 81.47 ± 4.5 % respectively in the AcH and AcM groups, compared with 71.67 ± 4.8 %, 68.81 ± 9.3 % and 67.85 ± 4.9 % in the AcL, Ac0, and Control groups, respectively (Fig. 5c and d).

3.6. Ac-containing hydrogel inhibited M1 polarization

During wound healing, inflammation, especially macrophage-induced response, initiates the entire healing cascade, which is important for tissue healing. To observe the inflammation level in diabetic wounds after different treatments, CD68 was used as a macrophage indicator, and iNOS and CD206 were used as M1 and M2 macrophage markers, respectively. Fig. 6a showed the immunofluorescence staining images of tissues in diabetic wounds after 7 days with different treatments. It could be observed that the green fluorescence (CD206) in the hydrogel groups was brighter than the Control group, and the red fluorescence (CD68), purple fluorescence (iNOS) in the Ac-containing hydrogel groups were darker than the Control and Ac0 groups. The corresponding statistical data in Fig. 6b and **c** showed that M1 macrophages were significantly decreased and M2 macrophages were significantly increased in the Ac-containing hydrogel groups compared with the Control group on day 7. After treatment for 14 days, the immunofluorescence staining images of macrophages at the wound site were shown in Fig. 6d. Compared with the other three groups, the green fluorescence (CD206) was significantly brighter and the purple fluorescence (iNOS) was significantly darker in the AcM and AcH groups. And quantitative results showed that the AcM and AcH groups had less M1 macrophages and more M2 macrophages than the other three groups (Fig. 6e and f). The above results indicated that the Ac-containing hydrogel groups could effectively reduce the inflammatory response at the diabetic wound sites.

3.7. Histological evaluation

HE staining, Masson staining, and CD31 immunohistochemical staining were applied to further evaluate the healing effect of hydrogel on wound tissues at day 14. As shown in Fig. 7a, the wound gap was indicated by two red triangles. The differences in the wound gap among the five groups were remarkable, with more intact epidermal tissue and smaller wound gaps in the AcH and AcM groups. The corresponding statistical measurements (Fig. 7b) showed that the wound healing effect was more significant with increasing Ac loading. The thickness of the epidermis regeneration is an important indicator to evaluate the effectiveness of wound healing. As shown in Fig. 7c, the regenerated epidermis in the Control group was thinner than the other hydrogel groups. Among the hydrogel groups, the regenerated epidermis produced in the AcH group showed a tendency to be thicker than the other three groups. Moreover, the statistics in Fig. 7d suggested that the AcH group also had more hair follicles than the other four groups. Fig. 7e showed the number of infiltrating neutrophils in the wound tissues. The hydrogel groups loaded wih Ac had decreased inflammatory cells, especially in the AcH group, while the Control group showed a large infiltration of inflammatory cells. Masson staining images and quantitative results showed that the collagen fibers density in tissues was the highest in the AcH group among the five groups, indicating better recovery of damaged tissue in the AcH group on day 14 (Fig. 7f and g). The formation of neovascularization is critical to ensure that nutrients and oxygen are transported to the wound site to improve the regeneration process. The immunohistochemical staining images of CD31 in tissues were shown in Fig. 7h, and the brown positive areas indicated the density of CD31. Compared with the Control group, the density of CD31 was higher on day 14 in the wound tissue of the hydrogel groups. The quantitative analysis (Fig. 7i) showed that the positive area of CD31 in the AcM and AcH groups was approximately 3 times that of the Control group, suggesting the formation of more mature capillaries in the AcM and AcH groups. In summary, the AcH hydrogel could promote wound repair through reducing inflammatory cells infiltration, accelerating wound contraction, and promoting collagen deposition and angiogenesis.

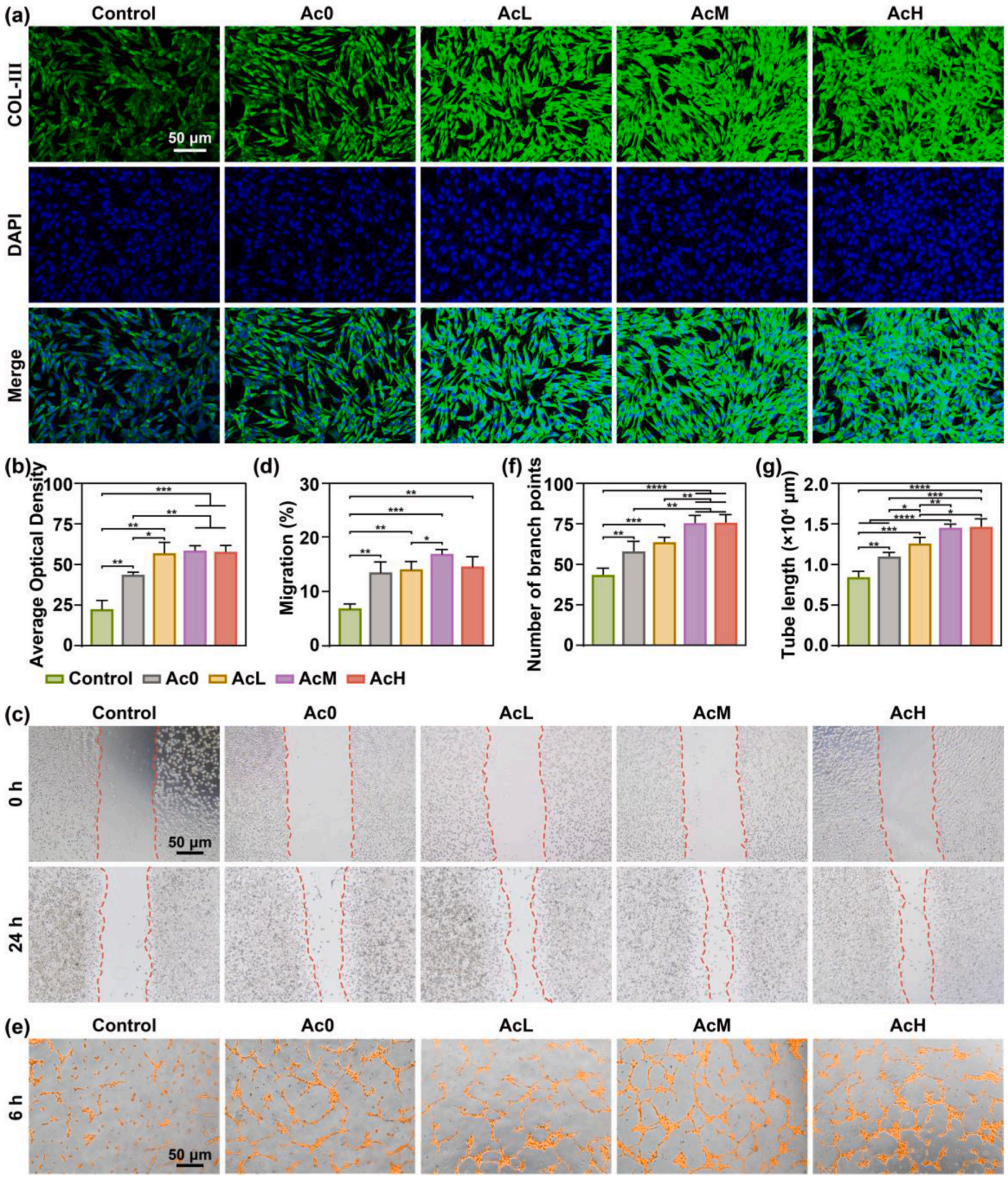

Fig. 3. Collagen secretion, cell migration, and angiogenesis of cells co-cultured with conditional medium *in vitro*. Representative images (a) and quantification of fluorescent intensity (b) of COL-III staining of L929 in Control, Ac0, AcL, AcM, and AcH groups under conditioned medium (The conditioned medium was derived from the supernatant of hydrogel cultured with macrophages for 4 days. n = 3). Representative images (c) and quantification (d) of L929 migration in Control, Ac0, AcL, AcM, and AcH groups under conditioned medium (n = 3). Representative images (e), number of branch points (f), and total tube length of the tube formation assay of HUVECs in Control, Ac0, AcL, AcM, and AcH groups under conditioned medium (n = 4). Data were presented by mean ± SD. P value was calculated by one-way ANOVA. *p < 0.05, **p < 0.01, ***p < 0.001, ****p < 0.0001.

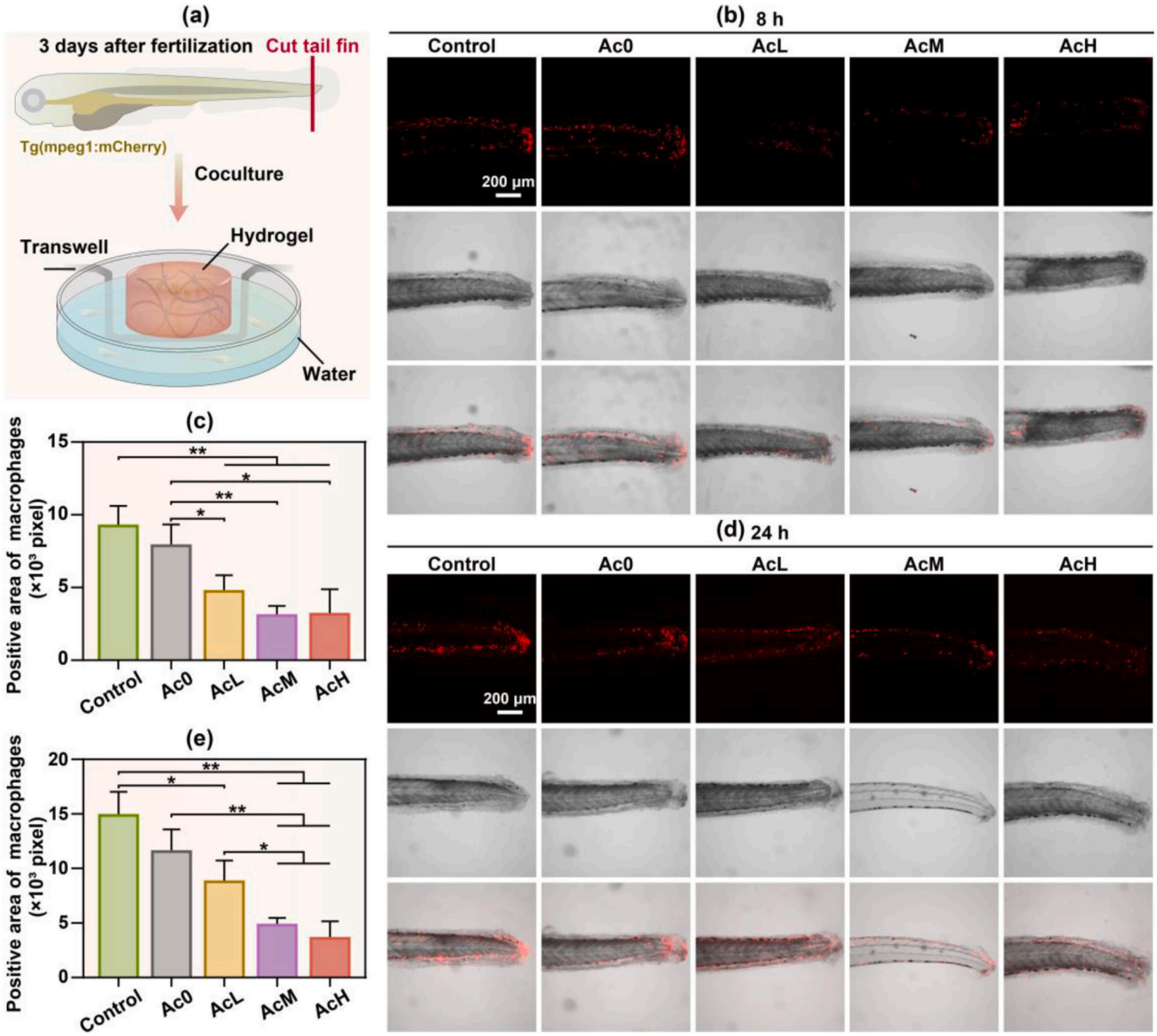

Fig. 4. Inflammatory response of hydrogel in zebrafish tail-breaking model. (a) Schematic diagram of the experimental process in zebrafish tail-breaking modeling. Representative fluorescence images (b) and statistics analysis of positive area (c) of macrophages in Control, Ac0, AcL, AcM and AcH groups after culture for 8 h. Representative fluorescence images (d) and statistics analysis of positive area (e) of macrophages in Control, Ac0, AcL, AcM and AcH groups after culture for 24 h. Data were presented by mean ± SD, n = 3. P value was calculated by one-way ANOVA. *p < 0.05, **p < 0.01.

3.8. RNA-Seq analysis

The mechanism of hydrogel in anti-inflammation was investigated by RNA-Seq, and the results were shown in Fig. 8. Transcripts with FPKM (Fragments Per Kilobase of gene per Million reads mapped) value ≥ 0 were included in our analysis. Based on their abundance, the total transcripts were divided into five categories, 0–0.25 FPKM, 0.25–0.5 FPKM, 0.5–1 FPKM, 1–10 FPKM, or ≥10 FPKM. Control and AcH samples had a similar distribution of expressed mRNAs (Fig. 8a). Fig. 8b and **c** showed that the bubble diagrams of KEGG enriched top 20 pathways of down-regulated and up-regulated genes, respectively. Compared with the Control group, the AcH hydrogel down-regulated nuclear factor kappa-B (NF-κB) signaling pathway and TNF signaling pathway, and up-regulated the signaling pathway about actin cytoskeleton, pentose phosphate pathway, and glycolysis/gluconeogenesis. Fig. 8d and **e** showed the enrichment score of the oxidative phosphorylation (OXPHOS) and heat map of genes in leading-edge subset expressed in AcH hydrogel versus Control group analyzed by GSEA based on the RNA-Seq datasets. AcH could up-regulate the OXPHOS, especially Cox10, Cox8b, Cox6a2, and Cox7a1 genes, compared with the Control group. Fig. 8f and **g** showed the enrichment score of the toll-like receptor (TLR) signaling pathway and heat map of genes in leading-edge subset expressed in AcH hydrogel versus Control group analyzed by GSEA based on the RNA-Seq datasets. AcH could down-regulate the TLR signaling pathway, especially TNF-α and IL-1β genes, compared with the Control group. The relative gene expression of TNF-α and IL-1β was further analyzed by RT-PCR and shown in Fig. 8h and i. AcH could significantly reduce expression of TNF-α and IL-1β compared with the Control. Moreover, the fluorescence intensity of NOD-like receptor thermal protein domain associated protein 3 (NLRP3) in macrophages of the AcH group was lower than that of the Control group (Fig. 8j). The above results suggested that the AcH could down-regulate the

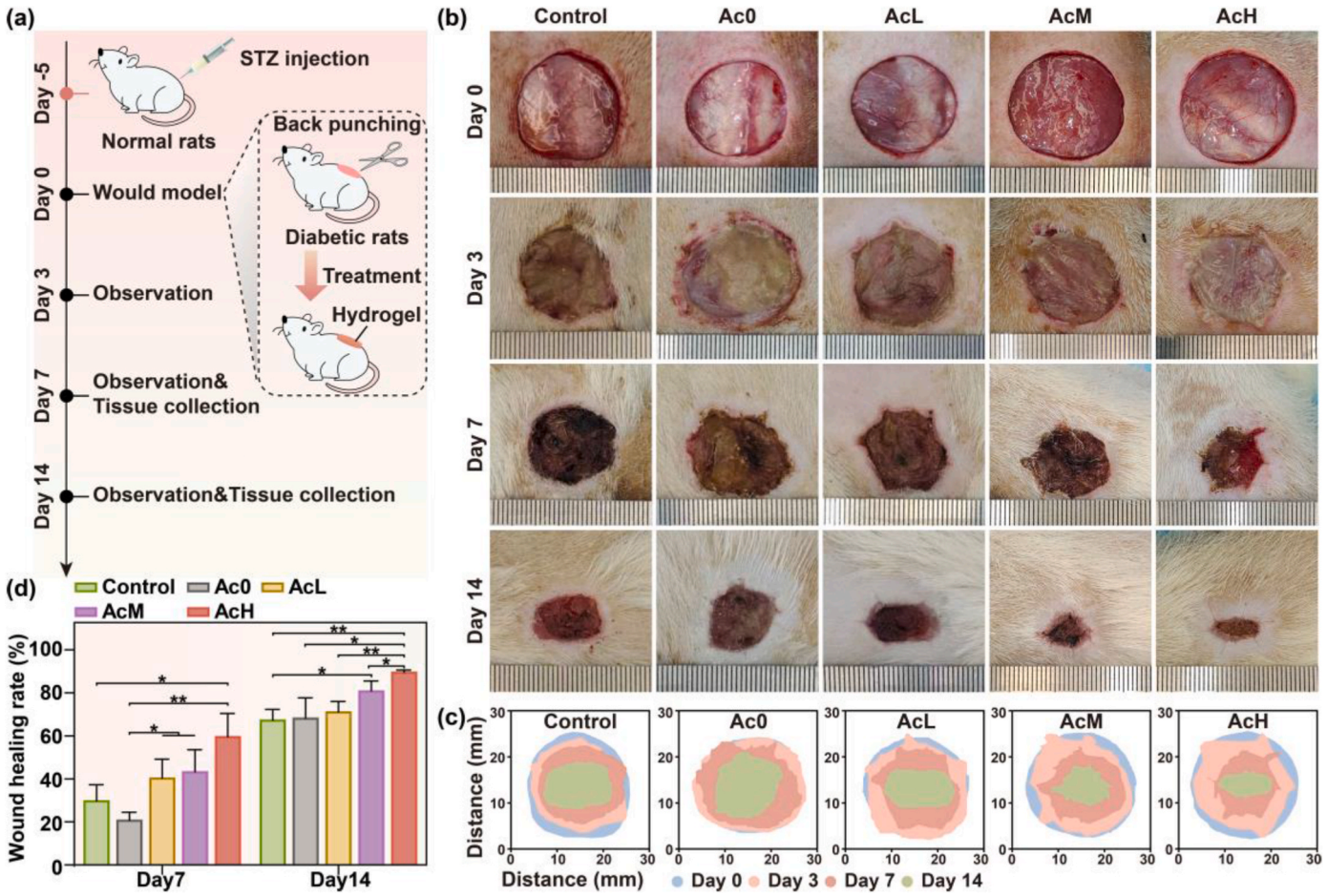

Fig. 5. Wound healing of hydrogel in a diabetic model. (a) Schematic diagram of the experimental processes in a diabetic wound model. (b) Representative images of the wounds in Control, Ac0, AcL, AcM and AcH groups on days 0, 3, 7, and 14. (c) Schematic diagram of the wound healing process with different treatments during 14 days. (d) Statistics of wound healing rate on day 7 and day 14 with different treatments. Data were presented by mean ± SD, n = 3. P value was calculated by one-way ANOVA. *p < 0.05, **p < 0.01.

inflammation-related signaling pathway to show a superior anti-inflammatory effect *in vivo*.

4. Discussion

In this work, β-CD was introduced into HA, and the two were bonded through hydrogen bonding, conjugated with drugs, and provide physical loading space in a cavity structure, so that polypeptide Ac could be stably loaded in the complex hydrogel.

Moreover, the addition of PVA and PEG could further enhance the cross-linking network of the hydrogel, to construct the complex hydrogel loaded with different concentrations of Ac. The complex hydrogel had excellent mechanical properties, self-healing properties, and skin adhesion, as well as had the biological function of anti-inflammation and promoting the healing of diabetic chronic wounds.

In diabetes, changes in the metabolic level of the organism can cause changes in the metabolic substrates and pathways of macrophages, thus disrupting their functional phenotypic transformation [30]. In the physiological environment, the polarization and efficient function of M1 macrophages depend on the glycolysis of glucose to provide energy, while the survival and activation of M2 macrophages mainly depend on the metabolism of glutamine in mitochondria, namely OXPHOS, and the oxidation of fatty acids to provide energy [31]. In diabetic patients, hyperglycemia causes an increased load on the mitochondrial electron transport chain (ETC), leading to OXPHOS dysfunction [32,33]. This leads to an insufficient supply of ATP, overproduction of reactive oxygen species (ROS), and imbalance of Ca^{2+} in and out of cells, thereby over-activating NLRP3 inflammasome and NF-κB, and promoting the release of inflammatory cytokines [34–37]. The results of over-activated M1 macrophages and the blocked polarization of the anti-inflammatory M2 type cause persistent inflammation [38]. Therefore, the recovery of OXPHOS activity in diabetic chronic wounds can help transformation of M2 macrophages and inhibit excessive inflammation.

OXPHOS drives ATP synthetase to synthesize ATP through the proton gradient produced by the ETC, thereby providing energy for anti-inflammatory conversion [39]. ETC consists of four enzyme complexes, including Complex I (NADH ubiquinone oxidoreductase/NADH dehydrogenase), Complex II (succinate ubiquinone oxidoreductase/succinate dehydrogenase), Complex III (ubiquinol cytochrome *c* oxidoreductase/cytochrome *bc*1 complex), and Complex IV (cytochrome *c* oxidase, COX). Cellular metabolic processes such as glycolysis, the tricarboxylic acid cycle (TCA), and β oxidation produce the reduced coenzymes NADH and FADH2, from which electrons are released and passed to oxygen through ETC, thereby gradually promoting ATP synthesis and release of energy. ROS such as superoxide anions and peroxides are also produced in this process [40,41]. During the Complex III reaction, coenzyme Q is reduced to a highly active semiquinone radical, an unstable substance that may lead to the "leakage" of electrons, directly transferring electrons to oxygen to form superoxide [42]. Complex IV, on the other hand, efficiently reduces oxygen to water, releasing very few reducing intermediates. Thus, the efficient operation of complex IV reactions is required to avoid the overproduction of ROS

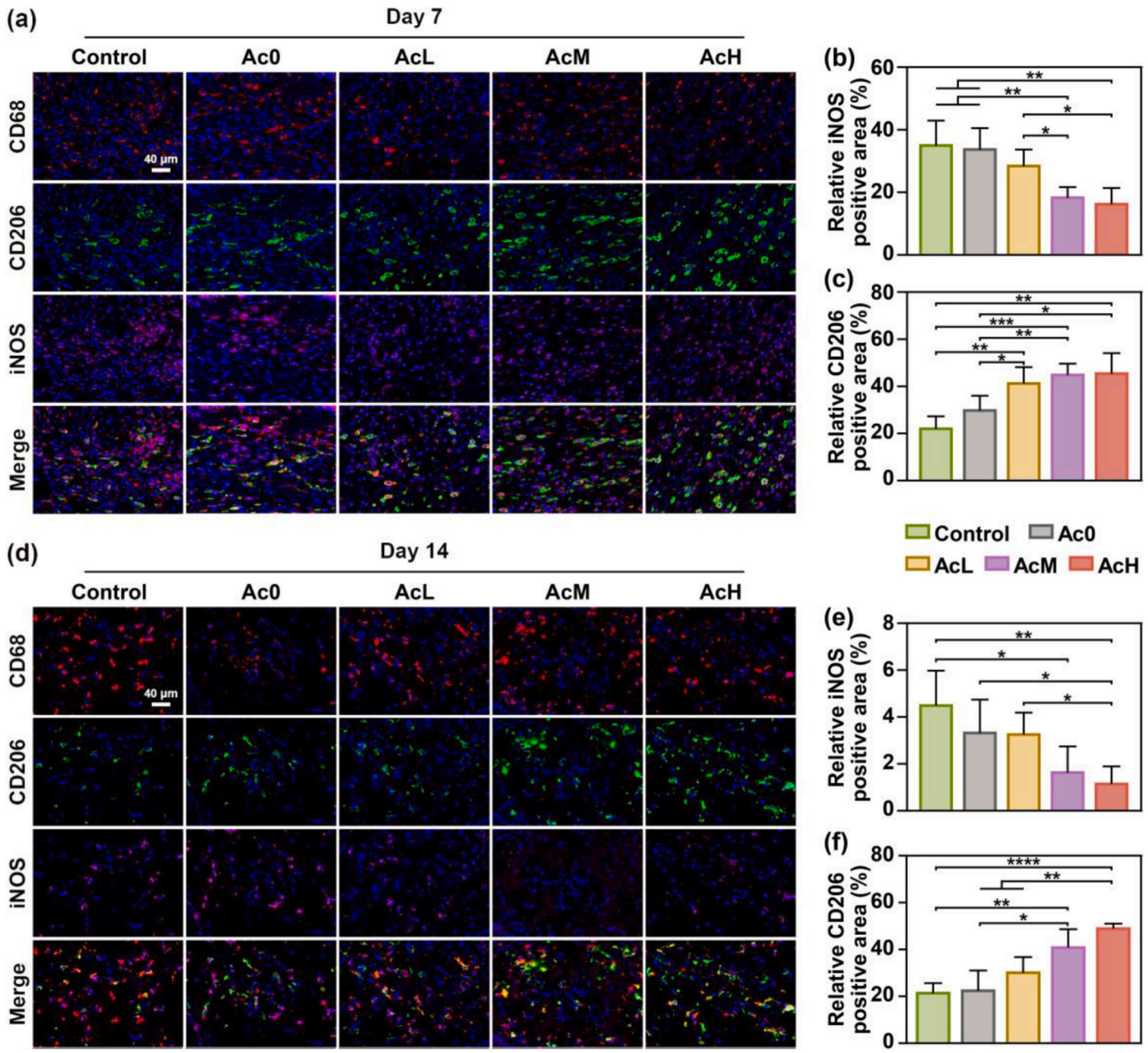

Fig. 6. Immune responses of tissues in a diabetic wound model. Immunofluorescence staining images (a) and relative positive area of iNOS (b) and CD206 (c) in tissues with different treatments on day 7. Immunofluorescence staining images (d) and relative positive area of iNOS (e) and CD206 (f) in tissues with different treatments on day 14. Data were presented by mean ± SD, n = 4. P value was calculated by one-way ANOVA. *p < 0.05, **p < 0.01, ***p < 0.001, ****p < 0.0001.

during OXPHOS [43]. In this work, compared with the untreated group, polypeptide complex hydrogel up-regulated the expression of COX-related genes, salvaged the OXPHOS damage in the hyperglycemic pathological environment, and thus promoted M2 polarization.

Subsequently, the anti-inflammatory immune environment is a favorable condition to promote the healing of diabetic wounds [44,45]. Diabetic wounds are difficult to heal due to immune system disorders and persistent inflammatory response [46]. However, the anti-inflammatory immune microenvironment is conducive to promoting the transformation of macrophages from M1 type to M2 type, reducing the expression of pro-inflammatory factors such as TNF-α and IL-1β, and promoting the expression of anti-inflammatory factors such as TGF-β1 and IL-10, so as to inhibit excessive inflammation and facilitate tissue repair [47–49]. At the site of injury, TLR can recognize both damage-associated molecular patterns (DAMPs) and pathogen-associated molecular patterns (PAMPs), further activate myD88-dependent pathways to activate NF-κB, and promote the release of inflammatory mediators and cytokines [50–52]. Polypeptide complex hydrogel down-regulated the TLR signaling pathway and decreased the expression of pro-inflammatory cytokines TNF-α and IL-1β, which inhibited the development of chronic inflammation. The complex hydrogel also promoted the release of IL-10 and TGF-β1 that improved collagen secretion, cell migration, and angiogenesis, which accelerated tissue healing. In summary, the complex hydrogel loaded with Ac polypeptide could promote M2 switch and alleviate excessive inflammation in diabetic wounds, which was a good candidate material for promoting chronic wound healing.

However, some challenges remain to be addressed. The dose of a drug is important for its biological effects, and the effects of a wider range of Ac2-26 concentrations on the inflammatory response and tissue

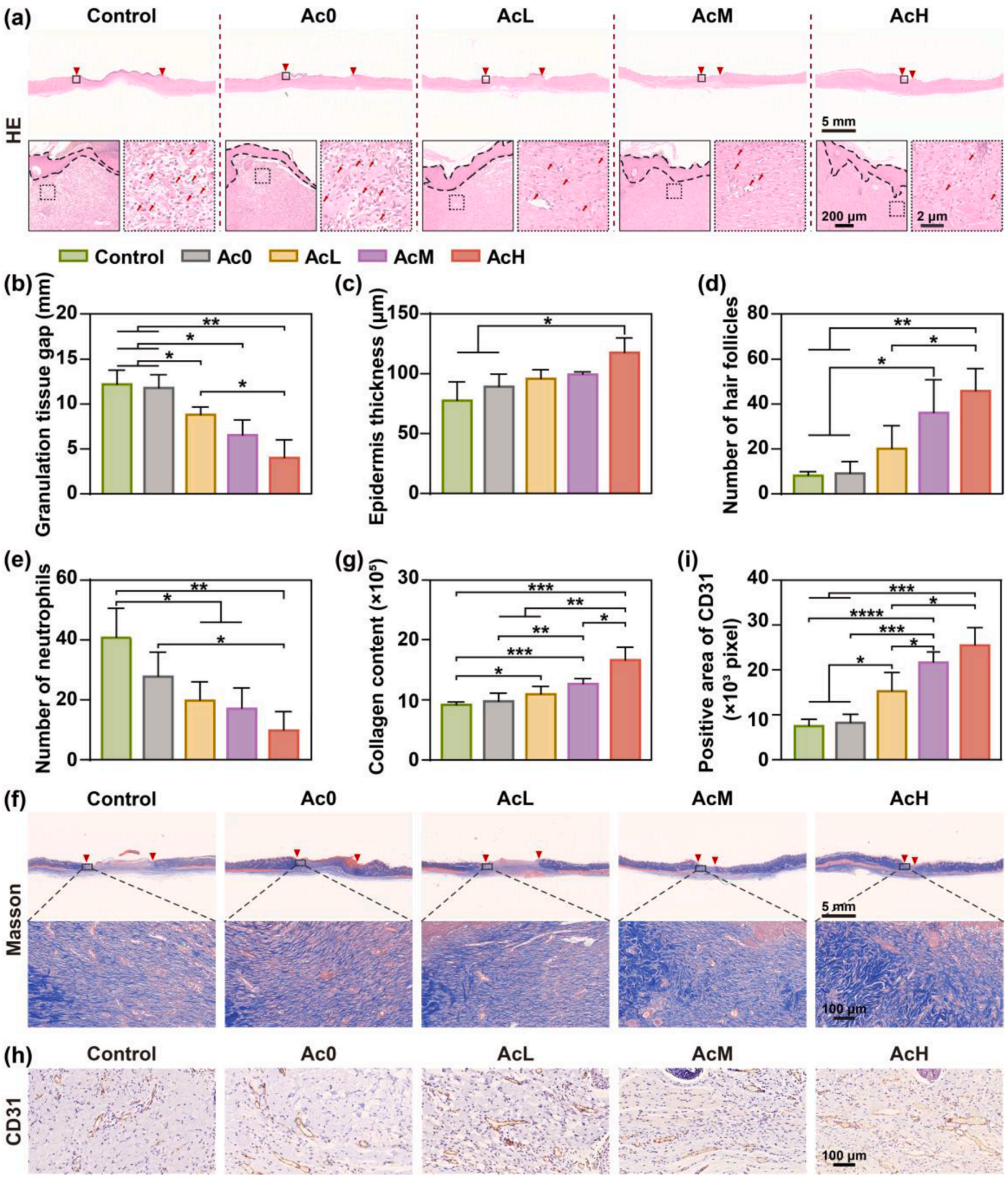

Fig. 7. Immunohistochemical analysis of wound tissues in different groups on day 14. (a) HE staining images of wound tissues in Control, Ac0, AcL, AcM and AcH groups on day 14 (Red triangles denote the areas of unhealed wounds; black dashed lines denote the regenerated epidermis; red arrows denote neutrophils). Statistics analysis of wound gap (b), epidermis thickness (c), number of hair follicles (d) and number of neutrophils (e) from HE staining images (n = 3). Masson staining images (f) and collagen content (g) of wound tissues in Control, Ac0, AcL, AcM and AcH groups on day 14 (n = 4). Immunohistochemical images (h) and positive area (i) of CD31 in wound tissues in Control, Ac0, AcL, AcM and AcH groups on day 14 (n = 4). Data were presented by mean ± SD. P value was calculated by one-way ANOVA. *p < 0.05, **p < 0.01, ***p < 0.001, ****p < 0.0001.

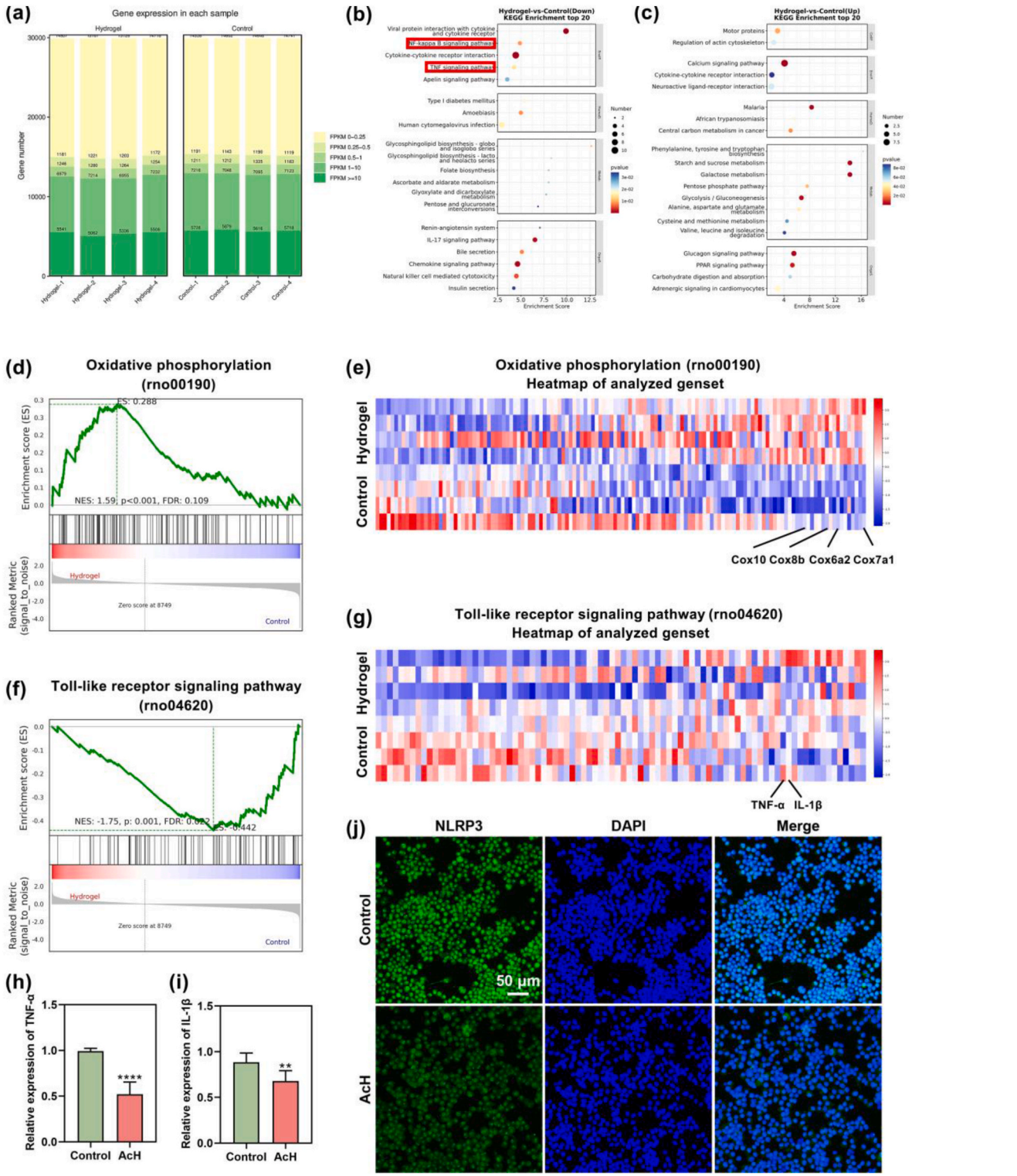

Fig. 8. The anti-inflammatory mechanism of hydrogel containing Ac. (a) Distribution of FPKM normalized transcripts of hydrogel and Control groups. (b) Bubble diagram of KEGG enriched top 20 pathways of down-regulated genes. (c) Bubble diagram of KEGG enriched top 20 pathways of up-regulated genes. (d) Enrichment score of the oxidative phosphorylation and (e) heat map of genes in leading-edge subset expressed in AcH hydrogel versus Control group analyzed by GSEA based on the RNA-Seq datasets. (f) Enrichment score of the TLR signaling pathway and (g) heat map of genes in leading-edge subset expressed in AcH hrdrogel versus Control group analyzed by GSEA based on the RNA-Seq datasets. (h) Relative expression of TNF-α (h) and IL-1β (i) genes in tissue of AcH and Control groups (n = 6). (j) Immunofluorescence staining images of NLRP3 in macrophages of AcH and Control groups. Data were presented by mean ± SD. P value was calculated by one-way ANOVA. **p < 0.01, ****p < 0.0001.

repair need to be systematically investigated. Moreover, whether HA complex hydrogel is the best carrier for Ac2-26 still needs to be considered. In addition, given the functional diversity of peptide drugs, it is clinically important to assess whether HA complex hydrogels can be used as a universal loading platform for peptide drugs.

5. Conclusions

Diabetic chronic wound healing poses a significant clinical challenge, in which the regulation of inflammation plays a key role. In this study, we successfully developed a hydrogel containing polypeptide (Ac) with good mechanical properties, self-healing properties, and skin adhesion. Moreover, the Ac-containing hydrogel could modulate the excessive inflammatory response of macrophages to stimulate collagen secretion, and promote cell migration and angiogenesis *in vitro*. RNA-Seq analysis showed that the hydrogel could restore the OXPHOS process, and down-regulate TLR signaling pathway, resulting in a significant anti-inflammatory effect. The *in vivo* evaluations confirmed that the hydrogel could modulate macrophage polarization and promote collagen deposition and neovascularization during the course of diabetic wound healing. In summary, the Ac-containing hydrogel showed promising potential in immunomodulation-based wound therapy and was effective in promoting diabetic wound healing.

CRediT authorship contribution statement

Ziyi Lu: Writing – original draft, Software, Methodology, Formal analysis, Data curation. **Kaijia Tan:** Writing – original draft, Software, Methodology, Formal analysis, Data curation. **Shuwen Xiang:** Data curation. **Yuchen Zhang:** Data curation. **Fangliang Luo:** Data curation. **Xingdan Liu:** Writing – review & editing. **Xiaoli Zhao:** Writing – review & editing, Project administration. **Liping Ouyang:** Writing – review & editing, Project administration, Funding acquisition, Conceptualization.

Declaration of competing interest

The authors declare that they have no known competing financial interests or personal relationships that could have appeared to influence the work reported in this paper.

Acknowledgements

Financial support from National Key Research and Development Program of China (2022YFC2403000), the National Natural Science Foundation of China (32371397, U21A20100), The Fundamental Research Funds for The Central Universities (YG2023ZD29), Research Fund of Shanghai Tongren Hospital, Shanghai Jiaotong University School of Medicine (2023DHYGJC-YBA01), and the Talent project of Shanghai Tongren Hospital (TRKYRC-xx02) are acknowledged.

Appendix A. Supplementary data

Supplementary data to this article can be found online at https://doi.org/10.1016/j.mtbio.2025.101690.

Supporting Information

Supplementary data to this article can be found online.

Data availability

Data will be made available on request.

References

[1] Y. Shou, Z. Le, H.S. Cheng, Q. Liu, Y.Z. Ng, D.L. Becker, et al., Mechano-activated cell therapy for accelerated diabetic wound healing, Adv. Mater. 35 (47) (2023) 2304638.
[2] M.G. Monaghan, R. Borah, C. Thomsen, S. Browne, You shall not heal: overcoming the non-healing behaviour of diabetic foot ulcers by engineering the inflammatory microenvironment, Adv. Drug Deliv. Rev. 203 (2023) 115120.
[3] X. Gao, M. He, W. Chen, Z. Wang, Y. Li, D. Bai, et al., Diabetic microenvironment-unlocked bioHJzyme with H_2S evolution for robust anti-pathogens and hyperinflammatory wound regeneration through TGF-β/Smad pathway, Adv. Funct. Mater. (2024) 2408236.
[4] C. Xing, H. Zhu, X. Dou, L. Gao, S. Baddi, Y. Zou, et al., Infected diabetic wound regeneration using peptide-modified chiral dressing to target revascularization, ACS Nano 17 (7) (2023) 6275–6291.
[5] G. Chen, Y. Yu, X. Wu, G. Wang, J. Ren, Y. Zhao, Bioinspired multifunctional hybrid hydrogel promotes wound healing, Adv. Funct. Mater. 28 (33) (2018) 1801386.
[6] M.-H. Fan, X.-Z. Zhang, Y.-L. Jiang, J.-K. Pi, J.-Y. Zhang, Y.-Q. Zhang, et al., Exosomes from hypoxic urine-derived stem cells facilitate healing of diabetic wound by targeting SERPINE1 through miR-486-5p, Biomaterials 314 (2025) 122893.
[7] M. Miao, Y. Niu, T. Xie, B. Yuan, C. Qing, S. Lu, Diabetes-impaired wound healing and altered macrophage activation: a possible pathophysiologic correlation, Wound Repair Regen. 20 (2) (2012) 203–213.
[8] M. Kloc, R.M. Ghobrial, J. Wosik, A. Lewicka, S. Lewicki, J.Z. Kubiak, Macrophage functions in wound healing, J Tissue Eng Regen Med 13 (1) (2019) 99–109.
[9] G.V. Ganesh, K.M. Ramkumar, Macrophage mediation in normal and diabetic wound healing responses, Inflamm. Res. 69 (4) (2020) 347–363.
[10] L. Zhao, H. Hu, L. Zhang, Z. Liu, Y. Huang, Q. Liu, et al., Inflammation in diabetes complications: molecular mechanisms and therapeutic interventions, MedComm 5 (4) (2024) e516.
[11] Y. Li, W. Zhang, R. Zhao, X. Zhang, Advances in oral peptide drug nanoparticles for diabetes mellitus treatment, Bioact. Mater. 15 (2022) 392–408.
[12] D. Fonseca Hernandez, L. Mojica, E. Gonzalez de Mejia, Legume-derived bioactive peptides: role in cardiovascular disease prevention and control, Curr. Opin. Food Sci. 56 (2024) 101132.
[13] K. Qian, P. Yang, Y. Li, R. Meng, Y. Cheng, L. Zhou, et al., Rational fusion design inspired by cell-penetrating peptide: SS31/S-14 G Humanin hybrid peptide with amplified multimodal efficacy and bio-permeability for the treatment of Alzheimer's disease, Asian J. Pharm. Sci. 19 (4) (2024) 100938.
[14] Y. Wu, Y. Wang, Z. Fu, H. Sun, Y. Liu, C. Li, et al., Peptide RL-QN15 promotes regeneration of epidermal nerve fibers and recovery of sensory function in diabetic skin wounds, FASEB J. 37 (4) (2023) e22892.
[15] Y. Li, Y. Ma, J. Yu, C. Li, D. Yu, R. Dai, et al., A dual functional polypeptide with antibacterial and anti-inflammatory properties for the treatment of periodontitis, Int. J. Biol. Macromol. 242 (2023) 124920.
[16] D. Wu, Y. Gao, Y. Qi, L. Chen, Y. Ma, Y. Li, Peptide-based cancer therapy: o pportunity and challenge, Cancer Lett. 351 (1) (2014) 13–22.
[17] K. Fosgerau, T. Hoffmann, Peptide therapeutics: current status and future directions, Drug Discov. Today 20 (1) (2015) 122–128.
[18] S. Yang, M. Wang, T. Wang, M. Sun, H. Huang, X. Shi, et al., Self-assembled short peptides: recent advances and strategies for potential pharmaceutical applications, Mater Today Bio 20 (2023) 100644.
[19] T. Kang, G.D. Cha, O.K. Park, H.R. Cho, M. Kim, J. Lee, et al., Penetrative and sustained drug delivery using injectable hydrogel nanocomposites for postsurgical brain tumor treatment, ACS Nano 17 (6) (2023) 5435–5447.
[20] X. Liu, Z. Guo, J. Wang, W. Shen, Z. Jia, S. Jia, et al., Thiolation-based protein–protein hydrogels for improved wound healing, Adv. Healthcare Mater. 13 (14) (2024) 2303824.
[21] X. Chen, X. Li, W. He, M. Wang, A. Gao, L. Tong, et al., Rational multivalency construction enables bactericidal effect amplification and dynamic biomaterial design, Innovation 4 (5) (2023).
[22] Z. Luo, Y. Wang, J. Li, J. Wang, Y. Yu, Y. Zhao, Tailoring hyaluronic acid hydrogels for biomedical applications, Adv. Funct. Mater. 33 (49) (2023) 2306554.
[23] A. Chhillar, A. Jaiswal, Hyaluronic acid-based self-healing hydrogels for diabetic wound healing, Adv. Healthcare Mater. (2024) e2404255.
[24] Z. Zhang, Y. Liu, X. Tao, P. Du, M. Enkhbat, K.S. Lim, et al., Engineering cell microenvironment using nanopattern-derived multicellular spheroids and photo-crosslinked gelatin/hyaluronan hydrogels, Polymers 15 (8) (2023) 1925.
[25] H.-Y. Lee, C.-H. Hwang, H.-E. Kim, S.-H. Jeong, Enhancement of bio-stability and mechanical properties of hyaluronic acid hydrogels by tannic acid treatment, Carbohydr. Polym. 186 (2018) 290–298.
[26] N. Lagneau, P. Tournier, B. Halgand, F. Loll, Y. Maugars, J. Guicheux, et al., Click and bioorthogonal hyaluronic acid hydrogels as an ultra-tunable platform for the investigation of cell-material interactions, Bioact. Mater. 24 (2023) 438–449.
[27] H. Liu, J. Chen, X. Li, Z. Deng, P. Gao, J. Li, et al., Amphipathic β-cyclodextrin nanocarriers serve as intelligent delivery platform for anticancer drug, Colloids Surf., B 180 (2019) 429–440.
[28] K.M. Sahu, S. Patra, S.K. Swain, Host-guest drug delivery by β-cyclodextrin assisted polysaccharide vehicles: a review, Int. J. Biol. Macromol. 240 (2023) 124338.
[29] X. Dong, J. Zhao, D. Jiang, Z. Lu, X. Liu, K. Tan, et al., Self-healing hydrogel reduces inflammation through ANT1/OPTN axis mediated mitophagy for spinal cord injury repair, Chem. Eng. J. 492 (2024) 152263.
[30] X. Qi, E. Cai, Y. Xiang, C. Zhang, X. Ge, J. Wang, et al., An immunomodulatory hydrogel by hyperthermia-assisted self-cascade glucose depletion and ROS

scavenging for diabetic foot ulcer wound therapeutics, Adv. Mater. 35 (48) (2023) 2306632.
[31] J. Blagih, G. Jones Russell, Polarizing macrophages through reprogramming of glucose metabolism, Cell Metab. 15 (6) (2012) 793–795.
[32] B.A. Al-Ghamdi, J.M. Al-Shamrani, A.M. El-Shehawi, I. Al-Johani, B.G. Al-Otaibi, Role of mitochondrial DNA in diabetes mellitus type I and type II, Saudi J. Biol. Sci. 29 (12) (2022) 103434.
[33] S. Hussain, A.W. Khan, A. Akhmedov, R. Suades, S. Costantino, F. Paneni, et al., Hyperglycemia induces myocardial dysfunction via epigenetic regulation of JunD, Circ. Res. 127 (10) (2020) 1261–1273.
[34] H. Ding, J. Li, Y. Li, M. Yang, S. Nie, M. Zhou, et al., MicroRNA-10 negatively regulates inflammation in diabetic kidney via targeting activation of the NLRP3 inflammasome, Mol. Ther. 29 (7) (2021) 2308–2320.
[35] Z. Cai, Y. Li, L. Bai, J. Xu, Z. Liu, T. Zhang, et al., Tetrahedral framework nucleic acids based small interfering RNA targeting receptor for advanced glycation end products for diabetic complications treatment, ACS Nano 17 (22) (2023) 22668–22683.
[36] B.K. Ziehr, J.A. MacDonald, Regulation of NLRPs by reactive oxygen species: a story of crosstalk, BBA - Molecular Cell Research 1871 (8) (2024) 119823.
[37] Y. Li, Q. Liang, L. Zhou, Y. Cao, J. Yang, J. Li, et al., An ROS-responsive artesunate prodrug nanosystem co-delivers dexamethasone for rheumatoid arthritis treatment through the HIF-1α/NF-κB cascade regulation of ROS scavenging and macrophage repolarization, Acta Biomater. 152 (2022) 406–424.
[38] Y. Qian, Y. Zheng, J. Jin, X. Wu, K. Xu, M. Dai, et al., Immunoregulation in diabetic wound repair with a photoenhanced glycyrrhizic acid hydrogel scaffold, Adv. Mater. 34 (29) (2022) 2200521.
[39] D. Vats, L. Mukundan, J.I. Odegaard, L. Zhang, K.L. Smith, C.R. Morel, et al., Oxidative metabolism and PGC-1beta; attenuate macrophage-mediated inflammation, Cell Metab. 4 (1) (2006) 13–24.
[40] I. Vercellino, L.A. Sazanov, The assembly, regulation and function of the mitochondrial respiratory chain, Nat. Rev. Mol. Cell Biol. 23 (2) (2022) 141–161.
[41] E. Sassetti, M.H. Clausen, L. Laraia, Small-molecule inhibitors of reactive oxygen species production, J. Med. Chem. 64 (9) (2021) 5252–5275.
[42] T. Homma, S. Kobayashi, H. Sato, J. Fujii, Superoxide produced by mitochondrial complex III plays a pivotal role in the execution of ferroptosis induced by cysteine starvation, Arch. Biochem. Biophys. 700 (2021) 108775.
[43] A. Aich, A. Boshnakovska, S. Witte, T. Gall, K. Unthan-Fechner, R. Yousefi, et al., Defective mitochondrial COX1 translation due to loss of COX14 function triggers ROS-induced inflammation in mouse liver, Nat. Commun. 15 (1) (2024) 6914.
[44] A.S. Kimball, F.M. Davis, A. denDekker, A.D. Joshi, M.A. Schaller, J. Bermick, et al., The histone methyltransferase setdb2 modulates macrophage phenotype and uric acid production in diabetic wound repair, Immunity 51 (2) (2019) 258, 71.e5.
[45] M. Kharaziha, A. Baidya, N. Annabi, Rational design of immunomodulatory hydrogels for chronic wound healing, Adv. Mater. 33 (39) (2021) 2100176.
[46] D. Lv, X. Cao, L. Zhong, Y. Dong, Z. Xu, Y. Rong, et al., Targeting phenylpyruvate restrains excessive NLRP3 inflammasome activation and pathological inflammation in diabetic wound healing, Cell Rep Med 4 (8) (2023) 101129.
[47] K. Boodhoo, D. de Swardt, C. Smith, M. van de Vyver, Ex vivo tolerization and M2 polarization of macrophages dampens both pro- and anti-inflammatory cytokine production in response to diabetic wound fluid stimulation, Biochimie 196 (2022) 143–152.
[48] Q.-Y. Zhang, H.-Y. Zhang, S.-G. Feng, M.-D. Yao, J.-J. Ding, X.-M. Li, et al., Macrophage metabolic reprogramming ameliorates diabetes-induced microvascular dysfunction, Redox Biol. 79 (2025) 103449.
[49] S. Maccari, E. Profumo, L. Saso, G. Marano, B. Buttari, Propranolol promotes monocyte-to-macrophage differentiation and enhances macrophage anti-inflammatory and antioxidant activities by NRF2 activation, Int. J. Mol. Sci. 25 (7) (2024) 3683.
[50] L. Zhang, Y. Sun, Z. Yang, P. Xia, Asarinin inhibits immunological rejection via the Toll-like receptor-myeloid differentiation factor 88 signaling pathway *in vitro*, Transpl. Immunol. 81 (2023) 101949.
[51] Z. Hu, D. Chen, P. Yan, F. Zheng, H. Zhu, Z. Yuan, et al., Puerarin suppresses macrophage M1 polarization to alleviate renal inflammatory injury through antagonizing TLR4/MyD88-mediated NF-κB p65 and JNK/FoxO1 activation, Phytomedicine 132 (2024) 155813.
[52] S.-B. Yoon, H. Hong, H.-J. Lim, J.H. Choi, Y.P. Choi, S.W. Seo, et al., A novel IRAK4/PIM1 inhibitor ameliorates rheumatoid arthritis and lymphoid malignancy by blocking the TLR/MYD88-mediated NF-κB pathway, Acta Pharm. Sin. B 13 (3) (2023) 1093–1109.